

Simulation of silicon nanoparticles stabilized by hydrogen at high temperatures

Alexander Y. Galashev

Received: 10 July 2009 / Accepted: 1 March 2010 / Published online: 18 March 2010
© Springer Science+Business Media B.V. 2010

Abstract The stability of different silicon nanoparticles are investigated at a high temperature. The temperature dependence of the physicochemical properties of 60- and 73-atom silicon nanoparticles are investigated using the molecular dynamics method. The 73-atom particles have a crystal structure, a random atomic packing, and a packing formed by inserting a 13-atom icosahedron into a 60-atom fullerene. They are surrounded by a “coat” from 60 atoms of hydrogen. The nanoassembled particle at the presence of a hydrogen “coat” has the most stable number (close to four) of Si–Si bonds per atom. The structure and kinetic properties of a hollow single-layer fullerene-structured Si₆₀ cluster are considered in the temperature range $10\text{ K} \leq T \leq 1760\text{ K}$. Five series of calculations are conducted, with a simulation of several media inside and outside the Si₆₀ cluster, specifically, the vacuum and interior spaces filled with 30 and 60 hydrogen atoms with and without the exterior hydrogen environment of 60 atoms. Fullerene surrounded by a hydrogen “coat” and containing 60 hydrogen atoms in the interior space has a higher stability. Such cluster has smaller self-diffusion coefficients at high temperatures. The fullerene stabilized

with hydrogen is stable to the formation of linear atomic chains up to the temperatures 270–280 K.

Keywords Cluster · Fullerene · Hydrogen · Nanoparticle · Silicon · Structure · Thermal stability · Molecular dynamics · Modeling and simulation

Introduction

Silicon is the most important semiconducting material in the microelectronics industry. If current miniaturization trends continue, minimum device features will soon approach the size of atomic clusters. In this size regime, the structure and properties of materials often differ dramatically from those of the bulk. For example, one has observed the luminescence in nanostructured silicon clusters (Hirschman et al. 1996). The prediction of the structures and properties of medium-size (10–100 atoms) Si_n clusters is of critical importance in understanding the transition from microscopic to macroscopic behavior of nanomaterials and their possible technological applications. The investigations on Si_n clusters (Yoo et al. 2003) have been directed by significant developments observed in the field of carbon clusters. Silicon clusters of five atoms form three-dimensional compact structures, while pure carbon clusters with ten or less atoms show linear and ring structures (Ferraro 2007). The

A. Y. Galashev (✉)
Ural Division, Institute of Industrial Ecology,
Russian Academy of Sciences, Sofia Kovalevskaya Str.,
20a, GSP-594, Yekaterinburg, Russia 620219
e-mail: galashev@ecko.uran.ru

structure of the C_{60} cluster, i.e., fullerene, is represented by a truncated icosahedron consisting of 20 hexagons and 12 pentagons that form a nearly spherical surface. Fullerene-like structures have not been identified for Si_n units; this is attributable to the sp^2 characteristic hybridization in fullerenes, which is more favorable for C_n than for Si_n units (Ferraro 2007). Theoretical models provide confirmation that the Si_{60} fullerene structure is more preferable than a network (naphthalene-like) structure or a cylinder structure. The fullerene structure of icosahedral symmetry has a local minimum at the potential energy surface. However, for silicon, this structure is unstable and experiences relaxation to the structure of “a ball with folds.” In general, a transformation of the atomic structure also occurs in this case, with the trend toward reconstruction of the tetrahedral atomic arrangement. Disregarding the instability of the Si_{60} fullerene structure, the authors of (Yu and Meyyappan 2006) calculated the electronic structure of Si_n and the changes in the electronic structure as a result of oligomerization. It was concluded that from an energetic standpoint, a large number of open and closed structures based on Si_n fullerene were possible. However, no methods for synthesizing this new family of compounds have been found yet. Absolute instability of fullerene Si_{60} has been specified by a method of density-functional theory (Sun et al. 2003).

Stability of neutral and ionic Si_{50} cluster was investigated by full-potential linear-muffin-tin-orbital molecular-dynamics (FP-LMTO-MD) method (Li et al. 2003). The neutral and charged fullerene cages relaxed into distorted structures resembling puckered balls. They were considerably less steady than the stacked structure built from tricapped trigonal prism (TTP). By comparison, for the fullerene cages and stacked structures of neutral and ionic Si_{60} cluster, similar characteristics were found. Also, stability of the hollow Si clusters of smaller size was investigated by the FP-LMTO-MD method. Calculations on the fullerene cage structures and the binding energies of Si_n ($n = 20, 24, 26, 28, 30, 32$) clusters were performed (Li and Cao 2001). It is found that the fullerene cages are not stable, and relax into structures which are severely distorted. Except for Si_{20} , their atomic arrangement tends toward tetrahedral geometry. After the structural distortion, about two silicon atoms can still be filled into the inside spaces of the distorted cages for Si_n ($n = 26–32$). Among

the selected 15 stable structures for Si_{20} , the most stable structure is constructed by stacking Si_9 TTP subunits (Li and Cao 2000).

As before there is an open question as to how one can obtain a smooth fullerene-like cage composed of Si atoms. Due to their sp^3 nature, the Si atoms do not tend to bind themselves to general fullerene cages. Si_N clusters (N up to ~ 50) usually favor compact forms which are completely different from fullerene cages (Honea et al. 1999; Ho et al. 1998). We have shown that the structure of a Si_{60} cluster in a fullerene cage is highly distorted even at not so high temperature and at the presence of hydrogen. There is a suggestion to construct Si clusters in fullerene-like cages with transition-metal atom doping (Hiura et al. 2001). First-principles calculation shows that tungsten (W) may be a good candidate for doping of fullerene-like Si cages and WSi_{12} and WSi_{14} clusters are energetically most favorable. Geometric and electronic structures of metal (M) atom doped silicon (Si) clusters, MSi_N ($M = Ti, Hf, Mo$ and W), using mass spectrometry, a chemical-probe method, and photoelectron spectroscopy have been studied in the work (Ohara et al. 2003). In the mass spectra for all of the mixed cluster anions MSi_N^- , both MSi_{15}^- and MSi_{16}^- were abundantly produced compared to their neighbors. Together with the result of the adsorption reactivity and photoelectron spectroscopy, it was revealed that one metal atom can be encapsulated inside a Si_N cage at $N \geq 15$.

A number of theoretical studies of small- to medium-sized, hydrogen-terminated silicon clusters have been performed in recent years. According to these calculations, lattice distortions enhance the photoluminescence intensity for partially dehydrogenated clusters, while further dehydrogenation ultimately decreases the photoluminescence intensity. Mass spectrometry has been used to probe the hydrogen-to-silicon ratios of hydrogen-terminated silicon clusters generated using a variety of methods. A wide range of $[H]/[Si]$ ratios have been observed, ranging from close to two to almost zero, depending on the conditions used to prepare the clusters (Rechtsteiner et al. 2001). Despite quite extensive experimental and theoretical studies, little is really known about the formation, structure, and stabilities of Si_nH_x clusters.

In this article, we investigated the temperature dependences of the physicochemical properties (including the structural and kinetic properties) of

silicon nanoparticles in the form of a fragment of a diamond-like lattice, a particle with a random atomic packing, as well as a nanoassembly formed by inserting a 13-atom icosahedron into a 60-atom fullerene. A compact nanoassembly is a structure with a clearly pronounced three, five, and sixfold symmetries. It is important to study how the temperature affects the bulk and surface structures of these three 73-atom silicon nanoparticles surrounded by 60 hydrogen atoms, and to gain insight into temperature variations in the structure of hollow silicon clusters placed in hydrogen environment. Hydrogen atoms can be both inside and outside the clusters.

Calculations

In essence, molecular dynamics calculations are computer calculations that make it possible to solve numerically the many-body problem in mechanics. In the model, the positions and velocities of atoms are represented as time functions. The microscopic behavior of a system is calculated by solving the differential equations of motion with the use of initial positions and velocities of atoms and interatomic interaction forces. Integration of the equations of motion was performed using the fourth-order Runge–Kutta method. The time step Δt was equal to 10^{-16} s.

The main results were obtained using a canonical ensemble. Some microcanonical calculations to check up reliability of the received results were executed also.

We consider a heat bath with fixed reference temperature T_0 , which can get by inserting stochastic and friction terms in the equations of motion (Résoibois and De Leener 1977)

$$m_i \dot{v}_i = F_i - m_i \gamma v_i + R_i(t), \tag{1}$$

where F_i is the systematic force and R_i is a Gaussian stochastic variable with zero mean and with intensity

$$\langle R_i(t)R_j(t + \tau) \rangle = 2m_i \gamma k T_0 \delta(\tau) \delta_{ij}. \tag{2}$$

The damping constant γ determines the strength of the coupling to the bath. This equation corresponds physically to frequent collision with light particles that form an ideal gas at temperature T_0 . Let us enter a time constant $\tau_T = (2\gamma)^{-1}$, then the scaling term for particle velocity is defined (Berendsen et al. 1984) as

$$\xi = \left[1 + \frac{\Delta t}{\tau_T} \left(\frac{T_0}{T} - 1 \right) \right]^{1/2}. \tag{3}$$

Thus the change in temperature per time step can be made exactly equal to $(T_0 - T)\Delta t/\tau_T$ by scaling: $v(t + \Delta t) \leftarrow \xi v(t + \Delta t)$.

The model we used in our simulations is given by the potentials proposed in works (Tersoff 1988, 1989; Mousseau and Lewis 1991; Kwon et al. 1992; Biswas and Hamman 1987). Tersoff (1988, 1989) proposed a new form of binding of two atoms in a model with due regard for many-atom correlations. The main idea is that, in real systems, the strength of each bond depends on the local environment, so that the bonds formed by an atom with many neighbors are weaker than those formed with several nearest neighbors. The Tersoff potential can be represented in the following form (Tersoff 1988, 1989):

$$U = \frac{1}{2} \sum_{i \neq j} V_{ij}, \quad V_{ij} = f_C(r_{ij}) [f_R(r_{ij}) + b_{ij} f_A(r_{ij})], \tag{4}$$

where r_{ij} is the distance between the i th and j th atoms, f_A and f_R are the attractive and repulsive pair potentials, respectively, and f_C is the smooth cut-off function. The potentials f_A and f_R in an explicit form are represented by the Morse potentials

$$f_R(r) = A e^{-\lambda_1 r}, \quad f_A(r) = -B e^{-\lambda_2 r}, \tag{5}$$

$$f_C(r) = \begin{cases} 1, & r < R - D_R \\ \frac{1}{2} - \frac{1}{2} \sin \left[\frac{\pi}{2} (r - R) / D_R \right], & R - D_R < r < R + D_R \\ 0, & r > R + D_R \end{cases} \tag{6}$$

The parameters A and B determine the repulsive and attractive forces, respectively. The parameters R and D_R are chosen in such a way as to include only the layer of the first nearest neighbors in the bulk structures of silicon, graphite, and diamond. The smooth cut-off function f_C decreases from 1 to 0 in the range $R - D_R < r < R + D_R$. The main feature of this potential is the presence of the term b_{ij} . The bonding force depends on the local environment and decreases when the number of neighbors is large. This behavior of the bonding is governed by the term b_{ij} , which increases or decreases the ratio between the attractive and repulsive forces according to the relationship

$$b_{ij} = \frac{1}{(1 + \beta^n \zeta_{ij}^n)^{1/2n}}, \quad (7)$$

where

$$f_C^H(r) = \begin{cases} 1, & r \leq 0.17 \text{ nm} \\ 0.5 + 0.5 \cos[(\pi/0.2)(r - 0.17)], & 0.17 < r < 0.19 \text{ nm} \\ 0, & r \geq 0.19 \text{ nm} \end{cases} \quad (10)$$

$$\zeta_{ij} = \sum_{k \neq i,j} f_C(r_{ij}) g(\theta_{ijk}) e^{[\lambda_3^3 (r_{ij} - r_{ik})^3]},$$

$$g(\theta) = 1 + \frac{c^2}{d^2} - \frac{c^2}{[d^2 + (h - \cos \theta)^2]}. \quad (8)$$

The term ζ_{ij} characterizes the effective coordination number of the i th atom, i.e., the number of the nearest neighbors. This number is determined with allowance made for the relative distance between two neighbors $r_{ij} - r_{ik}$ and the bond angle θ . The function $g(\theta)$ describes the dependence of the coordination number on the bond angle. The parameter d characterizes the rate of change of the function $g(\theta)$. The parameter c specifies the dependence of the force on the angle θ . The parameters of the potential V_{ij} were chosen by fitting the theoretical and experimental data obtained for real and hypothetical configurations. These data involved the bonding energy, the lattice constant, and

the bulk modulus. The parameters of the Tersoff potential used for silicon are presented in Table 1.

When simulating the Si–H interactions, there arises a problem of control of the univalence of hydrogen. Mousseau and Lewis (1991) simulated an amorphous Si–H system with the use of the approach based on different potentials describing the bonded and nonbonded S–H interactions. The molecular dynamics calculations within this approach appear to be very slow virtually at any finite temperature. Kwon et al. (1992) proposed the potential that describes the Si–H interactions in an arbitrary configuration without necessity of including bonded and nonbonded Si–H pairs. This potential consists of two parts, one of which describes the pair interactions and the other part represents the triple interactions. The Si–H two-particle potential is written in the form

$$V_{\text{Si-H}}^{(2)} = [A_1 \exp(-\lambda_1 r) + A_2 \exp(-\lambda_2 r)] f_C^H(r), \quad (9)$$

where f_C^H is the cut-off function given by the formula

The parameters A_1 , A_2 , λ_1 , and λ_2 obtained by fitting to the ab initio calculated energy of hydrogen on a silicon cluster (Tersoff 1989) are listed in Table 2. The two-particle potential described by formulas (9) and (10) leads to a minimum energy of -3.05 eV at $r = 0.15$ nm, which is in good agreement with the energy of the Si–H bond and the mean bond length in the Si–H amorphous system. This potential also results in a frequency of $2,023 \text{ cm}^{-1}$ for the stretching vibration mode of the Si–H bond, which also agrees well with the experimental frequency of this mode. The short-range character of the interaction is provided by the cut-off function f_C^H , which can be represented in the form of a simple smooth functional.

The three-particle potential, which is important for simulating the Si–H covalent interaction and stabilizing the tetrahedral structure of silicon, is written in the form (Biswas and Hamman 1987)

Table 1 Parameters of the Tersoff potential for silicon

<i>A</i> (eV)	<i>B</i> (eV)	λ_1 (nm ⁻¹)	λ_2 (nm ⁻¹)	λ_3 (nm ⁻¹)	<i>n</i>	<i>c</i>	<i>d</i>	<i>R</i> (nm)	<i>D_R</i> (nm)	β	<i>h</i>
1830.8	471.18	2.4799	1.7322	0	0.78734	1.0039×10^5	16.217	0.285	0.015	1.1×10^{-6}	-0.59825

Table 2 Parameters of the potentials of the Si–H и H–H interactions

<i>A</i> ₁ (eV)	<i>A</i> ₂ (eV)	λ_1 (nm ⁻¹)	λ_2 (nm ⁻¹)	<i>B_H</i> (eV)	α (nm ⁻²)	α_H (nm ⁻²)	<i>r</i> _{c1} (nm)	<i>r</i> _{c2} (nm)	μ_1 (nm)	μ_2 (nm)	ε (eV)	α_{HH}	<i>r_m</i> (nm)
1113.967	-700	27.801	23.616	22.6526	30.34373	60.334	0.39527357	0.18	0.0312058	0.02	0.147	15.20	0.19

$$V^{(3)}(r_{12}, r_{13}, \theta) = B_H \varphi_{1,2}(r_{12}) \varphi_2(r_{13}) \times \left(\cos \theta + \frac{1}{3} \right)^2 g_{c_{1,2}}(r_{12}) g_{c_2}(r_{13}). \tag{11}$$

The indices 1 and 2 correspond to the Si–Si and Si–H interactions, respectively. The radial functions $\varphi_1(r)$ and $\varphi_2(r)$ are defined as $\varphi_1(r) = \exp(-\alpha r^2)$ and $\varphi_2(r) = \exp(-\alpha_H r^2)$. The cut-off functions (g_{c_1} , g_{c_2}) are represented in the form $g_{c_{1,2}}(r) = \{1 + \exp[(r - r_{c_{1,2}})/\mu_{1,2}]\}^{-1}$. The parameters B_H , α , α_H , r_{c_1} , and μ_i are given in Table 2. The parameters B_H and α_H were obtained by fitting of the rocking mode (630 cm⁻¹) and bending mode (897 cm⁻¹) for H–Si bond in amorphous Si:H. This potential describes the Si–Si–H, H–Si–H, and Si–H–Si interactions. It should be noted that the lowest energy is achieved when the H atom is bound to one Si atom.

The used H–H repulsive potential in the form

$$V_{HH}^{(2)}(r) = \left[\frac{\varepsilon}{(1 - 6/\alpha_{HH})} \right] \times \left[\left(\frac{6}{\alpha_{HH}} \right) \exp \left[\alpha_{HH} (1 - r/r_m) \right] - \left(\frac{r}{r_m} \right)^6 \right]. \tag{12}$$

prevents nonphysical approach of hydrogen atoms to one another (Biswas and Hamman 1987). In this scheme, the formation of H₂ molecules is impossible. Only atomic hydrogen is included in the model. The parameters ε , α_{HH} and r_m are presented in Table 2.

In the initial packing composed of the fullerene with the inscribed extended icosahedron, there are five fullerene atoms located at the distance equal to the bond length $L_b = 0.24$ nm for each atom

positioned on the icosahedron surface (Galashev et al. 2007). For an atom of the icosahedron surface, the five nearest neighbors also lying on the icosahedron surface can be disregarded, because the distance to these atoms is ~ 1.9 times larger than the bond length L_b , and the distance from the icosahedron center to atoms on its surface is 1.8 times larger than the bond length L_b . The attraction of the fullerene by the icosahedron is provided by 60 bonds.

First three series of calculations were performed for Si₇₃ nanoparticles. Each Si₇₃ particle was placed in a virtual sphere of the same diameter. The radius of the sphere was chosen so that 60 hydrogen atoms located at a distance of no less than 0.22 nm from each other can be randomly positioned in the space between the particle and the surface of the sphere. Therefore, the initial density of the hydrogen “coat” was approximately equal to 42–45 kg/m³. It should be noted that the experimental density of liquid hydrogen at 20 K is approximately equal to 70 kg/m³. The initial temperature (35 K) exceeded the boiling temperature of real hydrogen (20 K), so that the hydrogen environment of the nanoparticle even in the first calculation was a dense gas. The duration of the calculations at each temperature was equal to 10⁶ time steps or 100 ps. The final atomic configuration obtained at a lower temperature served as the initial configuration for the subsequent calculations at a higher temperature. In the calculations, the temperature was increased in steps of ~ 90 K. The last calculations were carried out at a temperature of 1,560 K. In the first series of calculations, a fragment composed of a particular site with 72 nearest neighbors in the diamond lattice was used as the initial

configuration. In the initial state, the density of the crystalline nanoparticle corresponded to that of the macrocrystalline material. In the second series of calculations, a fragment with a random atomic packing served as the initial configuration. This configuration of the nanoparticle was produced by filling a spherical region of the corresponding radius with silicon atoms by using a random-number generator. In the initial state, the minimum distance between silicon atoms in the random packing did not exceed the minimum distance in the corresponding macrocrystal (0.235 nm). As a result (and also in view of a decrease in the time of filling the sphere), the initial nanoparticle had a looser atomic packing. The nanoparticle density was no higher than 0.6 of the density of the silicon nanocrystal. In the third series of calculations, the initial configuration of the nanoparticle was represented by the nanoassembly composed of a 60-atom fullerene into which a 13-atom icosahedron was inserted. The minimum distance between the atoms in this nanoassembly corresponded to the minimum distances between atoms in the silicon macrocrystal.

Five series of calculations were carried out for hollow silicon clusters. In each series of calculations, the initial state was specified by the temperature 10 K. The last calculation was conducted for the temperature 1,711 K. In the first series of calculations, fullerene consisting of 60 atoms served as the initial configuration. In this configuration, the minimal distance between the atoms (0.24 nm) was close to the corresponding parameter in the macroscopic Si crystal. In the second series of calculations, the initial configuration corresponded to fullerene with 30 hydrogen atoms placed inside. These H atoms were located in the straight lines connecting the center of mass of the fullerene with the centers of each second Si atom forming the fullerene. In every case, the distance between Si and H atoms was 0.18 nm. The third series of calculations for the fullerene began with the placing of 60 H atoms inside the fullerene in the manner described above. Before the beginning of the fourth and fifth series, the Si_{60} fullerene filled with 30 or 60 H atoms was placed in virtual spheres with the same diameter. The radius of the sphere was chosen in such a way that 60 H atoms spaced from each other and from Si atoms by a distance no shorter than 0.22 nm could be randomly placed into the space between the particle and the sphere. Thus, the

initial density of the hydrogen “coat” was 42–43 kg/m^3 .

Results and discussion

The influence of hydrogen on the stability of Si_{73} nanoparticles

The hydrogen “coat” has a clear stabilizing effect on the Si_{73} nanoparticle, but does not provide the retention of the structure at a high temperature and does not prevent the evaporation of Si atoms. A Si atom was considered to belong to the cluster if the atom was linked to the cluster by at least one Si–Si bond. To identify the Si–Si bond at every time step, we checked whether each of the Si atoms was separated from the other Si atoms by a distance $r > r_{\text{max}} = 0.3$ nm. The linkage between the Si atom and the cluster was considered to be lost if this atom was separated from the other Si atoms by a distance larger than the radius of the second coordination sphere for silicon macrocrystal ($r_2 = 0.38$ nm). The cluster never joins the Si atom again if this atom is at a distance $r > r_2$ from the nearest neighboring atom. Evaporated atoms had a rather high relative kinetic energy and did not return to the clusters. Figure 1 depicts the configurations of the Si_{73} nanoassembled clusters after a 17-fold stepwise increase in the temperature, so that their kinetic energy approximately corresponds to a temperature of 1,560 K. It can be seen from Fig. 1a that, in the absence of hydrogen, the Si_{73} cluster has strongly expanded and lost five atoms by the instant of time 100 ps ($T = 1560$ K), two of which are shown in the lower

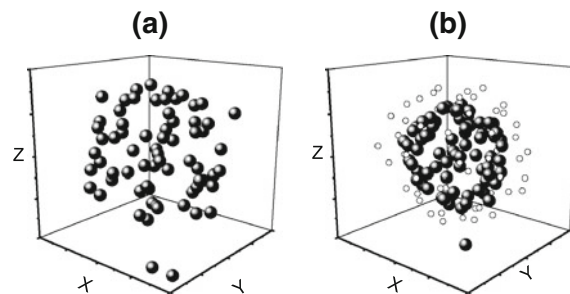


Fig. 1 Configurations of the Si_{73} cluster composed of a 13-atom icosahedron and a 60-atom fullerene: **a** cluster with a free surface and **b** cluster surrounded by 60 hydrogen atoms at the instant of time $t = 100$ ps and the temperature $T = 1560$ K

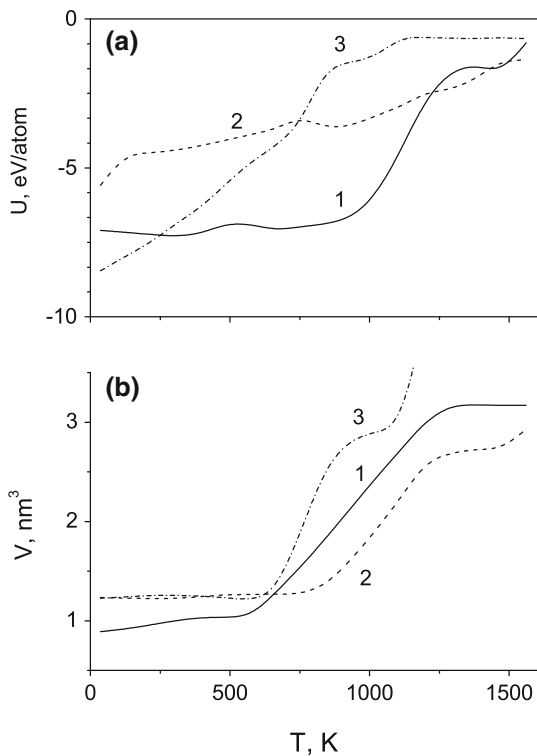


Fig. 2 Temperature dependences of **a** the internal energy of silicon clusters and **b** the volume of the virtual sphere bounding all atoms in the system: (1) nanoassembled particle, (2) nanocrystal, and (3) particle with a random atomic packing

part of Fig. 1a. In the presence of the hydrogen “coat” (Fig. 1b), the silicon cluster composed of the fullerene and the icosahedron even at this high temperature retains a spherical shape and only one of its atoms evaporates (this atom is shown in the lower part of Fig. 1b). Although the silicon cluster surrounded by hydrogen is expanded, its expansion is less pronounced than that of the cluster in the absence of the hydrogen “coat”.

The internal energy of the Si₇₃ cluster in the form of the diamond lattice fragment surrounded by the hydrogen “coat” smoothly increases from −5.18 eV/atom at 35 K to −2.65 eV/atom at 1560 K (Fig. 2a). The other two Si₇₃ clusters surrounded by hydrogen have stronger temperature dependences of the internal energy. In this case, the internal energy *U* for the nanoassembled cluster retains values comparable to those of crystalline silicon (−4.36 eV/atom) (Yin and Cohen 1982) up to a temperature of 1,112 K (−4.33 eV/atom). The internal energy of the cluster with the random packing rapidly increases with an

increase in the temperature, especially in the temperature range 690 ≤ *T* ≤ 850 K. At *T* = 750 K, the internal energy of this cluster reaches the internal energy *U* for the Si₇₃ nanocrystal. This behavior of the internal energy *U* is associated with the considerable transformation of the cluster structure. The particle with the random atomic packing, the nanoassembled particle, and the nanocrystal each lose one Si atom at temperatures of 760, 850, and 1,120 K, respectively. The internal energy *U* at temperatures above these values was determined for Si₇₂ clusters.

The temperature dependences of the volume of the sphere that is constructed from the center of mass of the cluster and contains all 73 atoms (including evaporated atoms) are plotted in Fig. 2b. The volume of the bounding sphere for the nanoassembled cluster and the cluster with the random atomic packing is retained (accurate to within 20%) only to a temperature of ~600 K, whereas the volume of the sphere circumscribed around the nanocrystal is retained (accurate to within 3%) up to a temperature *T* ~750 K. The atom is completely detached from the cluster (the Si–Si bonds of this atom with the cluster disappear completely) at higher temperatures.

Structure of Si₇₃ nanoparticles in the presence of hydrogen on their surface

The Si–Si covalent bond is a short-range bond. The cut-off function *f_C(r)* defined by expression (6) cuts off the Si–Si pair interactions at distances exceeding 0.3 nm. Let us assume that the criterion for the existence of the Si–Si bond is represented by the condition *r*_{Si–Si} < 0.3 nm. By using this criterion for the determination of distances *r*_{Si–Si} between the current Si atom and all the other Si atoms in the cluster, it is possible to calculate the mean number \bar{n}_b of bonds per atom and the mean length \bar{L}_b of the Si–Si bonds. The calculated values of \bar{n}_b and \bar{L}_b for the Si₇₃ clusters in the temperature range 35 ≤ *T* ≤ 1,560 K are presented in Fig. 3. At low temperatures (*T* < 630 K), the values of \bar{n}_b and \bar{L}_b for the nanoparticle with the random atomic packing are larger than those for the other clusters under consideration. These parameters for all the clusters under investigation decrease with an increase in the temperature. Upon heating by 1,525 K, the mean number \bar{n}_b of bonds in the cluster with the random atomic packing decreases most drastically (by

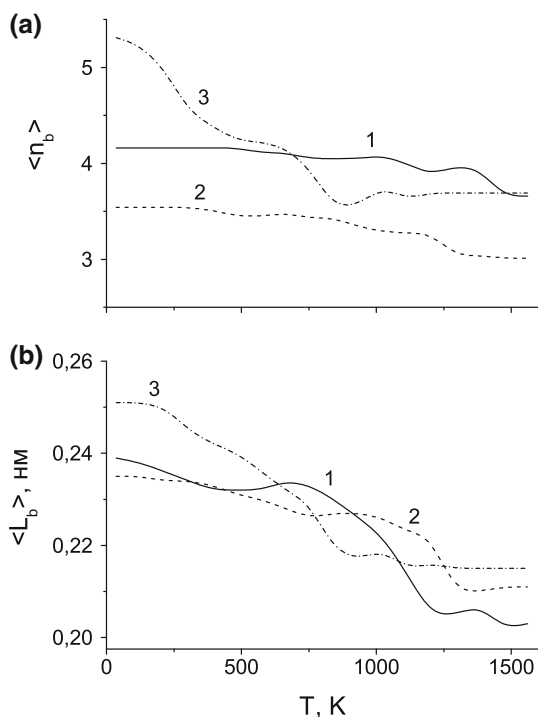


Fig. 3 Temperature dependences (canonical ensemble) of **a** the mean number of Si–Si bonds per atom in Si_{73} clusters and **b** the mean length of these bonds. The number designations are the same as in Fig. 2

approximately 30%). The mean numbers \bar{n}_b of bonds in the nanoassembled cluster and the nanocrystal decrease by 12 and 17%, respectively. It should be noted that, at temperatures above 690 K, the values of \bar{n}_b for the nanoassembled particle, as a rule, are larger than those for the other particles under investigation. The nanocrystal has the smallest values of \bar{n}_b over the entire temperature range.

At a temperature of 35 K, the mean bond length \bar{L}_b for the particles with noncrystalline packings is larger than the mean bond \bar{L}_b^{cryst} for the silicon crystal (0.235 nm). The equality $\bar{L}_b = \bar{L}_b^{\text{cryst}}$ is observed at $T = 250$ K for the nanoassembled particle and $T = 592$ K for the particle with the random atomic packing. Upon heating to 1,560 K, the mean bond lengths \bar{L}_b for the nanoassembled nanoparticle, the nanocrystal, and the particle with the random atomic packing decrease by 15, 10, and 14%, respectively. The mean bond lengths \bar{L}_b for the particle formed by inserting the icosahedron into the fullerene and the particle with the random atomic packing decrease most rapidly in the ranges $710 \leq T \leq 1,230$ K and

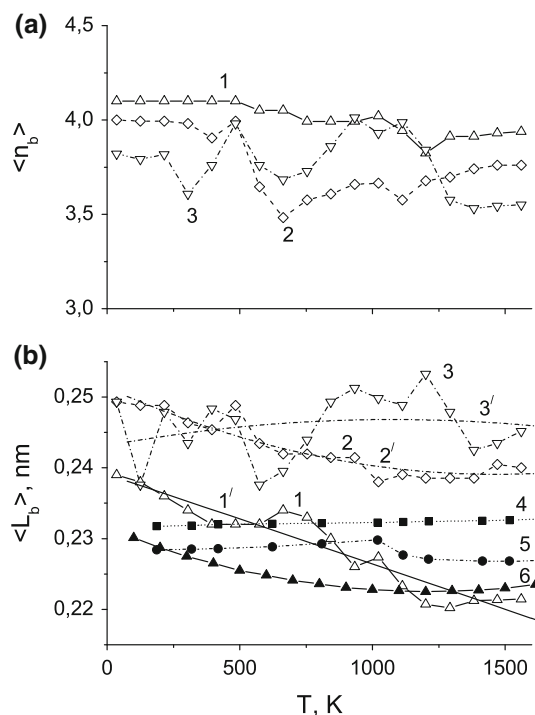


Fig. 4 Temperature dependences (microcanonical ensemble) of **a** the mean number of Si–Si bonds per atom in Si_{73} clusters and **b** the mean length of these bonds; (1) nanoassembled particle, (2) nanocrystal, and (3) particle with a random atomic packing; (1')–(3') are an approximation of the (1)–(3) dependences by polynom of the second degree. (4)–(6) are temperature dependences of the average distance $\bar{r}_{\text{Si-Si}}$ between the nearest neighbours in crystal (4), amorphous (5), and supercooled liquid (6) silicon

$170 \leq T \leq 890$ K, respectively. As a result, the smallest mean bond lengths \bar{L}_b at $T > 1090$ K are observed for the particle composed of the fullerene and the icosahedron. At $T > 1260$ K, the mean bond lengths \bar{L}_b for the nanocrystal again become smaller than those of the particle with the random atomic packing.

Mean numbers \bar{n}_b of bonds per atom and mean lengths \bar{L}_b of the Si–Si bonds for Si_{73} nanoparticles calculated using microcanonical ensemble are plotted in Fig. 4. Values \bar{n}_b of the nanoassembled particle poorly change with growth of temperature. The magnitude \bar{n}_b for this particle first decreases, but after temperature ~ 1200 K, starts to be increased. Nanoassembled particle has higher values \bar{n}_b in comparison with others considered nanoparticles up to temperature 930 K. Values \bar{n}_b for nanocrystal up to temperature 480 K and after temperature 1,280 K are higher than values of this magnitude for the

nanoparticle with the random atomic packing. With growth of temperature the \bar{n}_b magnitude for nanocrystal tends to increase at ~ 660 K. Dependence $\bar{n}_b(T)$ for the nanoparticle with the random atomic packing is characterized by the strongest fluctuations. However, in this case, the \bar{n}_b magnitude is inclined to small growth at $T > 1380$ K. Nevertheless, at heating from 35 K up to 1,560 K values, \bar{n}_b for the nanoassembled particle, the nanocrystal and the nanoparticle with the random atomic packing were reduced to 3.9, 6.0 and 7.0%, respectively. The reduction of magnitude \bar{n}_b observed in Si_{73} nanoparticles at the temperature increase is due to the fact that on average Si–Si bonds in them are weaker than in bulk silicon where the distance between the nearest neighbors is less than that in nanoparticles.

Mean length of the Si–Si bond for considered nanoparticles as a whole decreases with growth of temperature. The magnitude \bar{L}_b decreases for a nanoassembled particle by 10.0%, for a nanocrystal by 3.6%, and for a nanoparticle with a random atomic packing by 1.6%. This happens for the temperature range $35 \leq T \leq 1,560$ K. The nanoassembled particle has the lowest value \bar{L}_b at high temperatures, and the nanoparticle with the random atomic packing, the highest value. Fast decrease of the \bar{L}_b value for the nanoassembled particle begins at temperature ~ 660 K. At high temperatures, the \bar{L}_b value stops to be reduced because of amplifying repulsion between atoms. For the nanoassembled particle it occurs at 1,290 K, for the nanocrystal at 1,020 K, and for the nanoparticle with the random atomic packing at 13,80 K.

Data for amorphous silicon is of scientific interest because bulk amorphous silicon cannot be produced in real life. Amorphous silicon is prepared in the form of a thin film most that commonly uses plasma enhanced chemical vapour deposition. To obtain the structure of silicon equilibrated at 0.1 MPa and various other temperatures, MD simulation was carried out during heating and cooling cycles using NPT ensemble (Endo et al. 2003/2007). The unit cell used in this MD simulation contained 1,000 silicon atoms arranged in a diamond structure to which three-dimensionally periodic boundary condition was applied. Calculation was conducted at temperatures between 100 and 2,500 K. The melting point (1,768 K) estimated is higher than the experimental melting point (1,683 K) of silicon. This difference is

because silicon in the simulation has no surfaces serving as nucleation sites of melting.

On the basis of the data on density of work (Endo et al. 2003/2007) we have defined average distance $\bar{r}_{\text{Si-Si}}$ between the nearest neighbours in crystal and amorphous silicon in a temperature range $100 \leq T \leq 1,560$ K. The received dependences $\bar{r}_{\text{Si-Si}}(T)$ are shown by curves 4 and 5 in Fig. 4b. It is visible, that with growth of temperature, the magnitude $\bar{r}_{\text{Si-Si}}$ for crystal silicon is continuously increased. At initial heating of amorphous silicon (up to 1,000 K), the magnitude $\bar{r}_{\text{Si-Si}}$ increases, and at further increase of temperature, the values of $\bar{r}_{\text{Si-Si}}$ decrease. As a whole, at the temperature of 1,460 K, the value $\bar{r}_{\text{Si-Si}}$ for crystal silicon increases by approximately 0.5%, and for amorphous silicon, on the contrary, decreases by $\sim 0.7\%$.

Precise measurements of the density of supercooled liquid silicon using an electromagnetic levitation technique with static magnetic fields as well as first-principles molecular dynamics simulation of supercooled Si have been performed in work (Watanabe et al. 2007). A curve 5 in Fig. 4b shows that at high temperatures, in the absence of crystal order, the structural reorganizations in bulk silicon accompanied by reduction of average interatomic distance can take place. Average distances $\bar{r}_{\text{Si-Si}}$ between the nearest neighbours, received on the basis of extrapolation of these data in the area of low temperatures are plotted on the curve 6 in Fig. 4b. The minimal value of magnitude $\bar{r}_{\text{Si-Si}}$ (or the maximal value of density) for supercooled Si falls to the temperature 1,200 K. It is visible from Fig. 4b, that dependences $\bar{L}_b(T)$ for silicon nanoparticles under consideration fluctuate significantly. Significant fluctuations of magnitude \bar{L}_b are attributed to the fact that potential energy U of atoms on the surface of a nanoparticle essentially exceeds the magnitude U of the atoms in the nucleus of a cluster. Curves 1'–3' in Fig. 4b show approximations of dependences 1–3 by polynoms of a second degree. According to the smoothed dependences 1'–3', the magnitude \bar{L}_b in the interval $35 \leq T \leq 1,560$ K has decreased by 8.2% for nanoassembled particles and by 4.3% for nanocrystals, and for a particle with random atomic packing it has increased by 0.9%. Extrapolated dependence 6 for the supercooled liquid silicon shows, that the $\bar{r}_{\text{Si-Si}}$ magnitude is reduced by 2.8% at heating from 35 up to 1,560 K. Thus, among considered in this study

nanoparticles silicon nanocrystals have the closest dependence $\bar{L}_b(T)$ to the curve $\bar{r}_{\text{Si-Si}}(T)$ for the supercooled liquid silicon. However, the dependence $\bar{L}_b(T)$ for nanocrystals, on average in this figure, is 0.018 nm above the dependence $\bar{r}_{\text{Si-Si}}(T)$ for the supercooled liquid silicon.

Comparing curves 1–3, it is possible to conclude that Tersoff potential provides more correct description of the change of magnitude \bar{L}_b with the increase of temperature only in the case of the Si_{73} crystal nanoparticle, i.e., at the presence of the tetrahedral order of atoms. In this case, reduction of magnitude \bar{L}_b stops at $T > 1,200$ K, but its value for nanoparticle is still appreciably higher than the magnitude $\bar{r}_{\text{Si-Si}}$ for a macrocrystal (by 2.5%). At random packing of atoms in nanoparticle Si_{73} the magnitude \bar{L}_b increases with the temperature, and its divergence from the $\bar{r}_{\text{Si-Si}}$ for amorphous and supercooled liquid silicon amplifies. The magnitude \bar{L}_b for nanoassembled particle reduces very quickly at heating, and therefore its values at $T > 1,140$ K are even lower than the value $\bar{r}_{\text{Si-Si}}$ for the supercooled liquid silicon.

The tetrahedral coordination of Si atoms grows with decreasing temperature. The growing tetrahedral network would increase the number of nucleation sites, and thus, the nucleation rate would also be increased. Therefore, in the highly supercooled liquid, tetrahedrally coordinated atoms would make it difficult to form bulk amorphous Si from the supercooled liquid state. However, if we achieve a highly supercooled liquid state below 1,200 K, the liquid state has a high density, and therefore will be able to form bulk amorphous Si from this liquid state.

Owing to the strong directed short-range interactions the magnitude of a surface tension for silicon nanoparticles does not decrease with the growth of their size as it usually takes place for the majority of substances (Hawa and Zachariah 2004). Therefore, reduction of rigidity of the Si–Si bonds with growth of temperature can result in a reduction of the size of Si-cluster, i.e., the magnitude \bar{L}_b can be reduced due to forces of surface tension.

Calculations those use microcanonical ensemble give weaker temperature change of magnitudes \bar{n}_b and \bar{L}_b . Here reduction of function $\bar{L}_b(T)$ is not so essential, as during modeling in canonical ensemble. The best agreement of magnitudes \bar{n}_b and \bar{L}_b (the divergence on average is 2.0 and 2.6% respectively) in two different ensembles is observed for

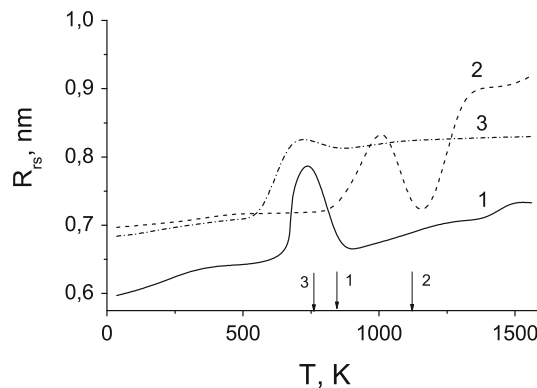


Fig. 5 Temperature dependences of the restricting sphere radius for silicon clusters. The number designations are the same as in Fig. 2. Arrows indicate the temperatures of the onset of evaporation of Si atoms from clusters

nanoassembled nanoparticle. The greatest ensemble divergence between these magnitudes is received for nanocrystal (12.8 and 7.9% for \bar{n}_b and \bar{L}_b respectively). In case of a particle with random atomic packing, the ensemble error for \bar{n}_b and \bar{L}_b is 11.2 and 8.6% respectively.

The restricting sphere radius R_{rs} is defined as the length of the segment from the center of the mass of the cluster to the center of the Si atom that is most distant from the cluster, but its distance to the nearest atom in the cluster should be no more than r_2 . The temperature dependences of the radius R_{rs} for the particles under consideration are plotted in Fig. 5. The dependences $R_{\text{rs}}(T)$ for the particles reflect the evaporation of atoms from the solid cluster. The peak in the dependence $R_{\text{rs}}(T)$ for the Si_{73} cluster with the random atomic packing is observed at the lowest temperature. This peak indicates that the atom evaporates from the particle. A similar peak for the nanoassembled cluster appears at a higher temperature. The corresponding peak in the dependence $R_{\text{rs}}(T)$ for the nanocrystal occurs at the highest temperature. The arrows near the abscissa axis indicate the temperatures of the onset of evaporation. The evaporation begins at a somewhat higher temperature T than the temperature at which the peak is located in the corresponding dependence $R_{\text{rs}}(T)$ due to the discreteness of the change in the temperature. The detachment of the atom from the cluster leads to a decrease in the cluster radius R_{rs} because the number of atoms contained in the cluster becomes smaller by unity. At a temperature of 1,560 K, the

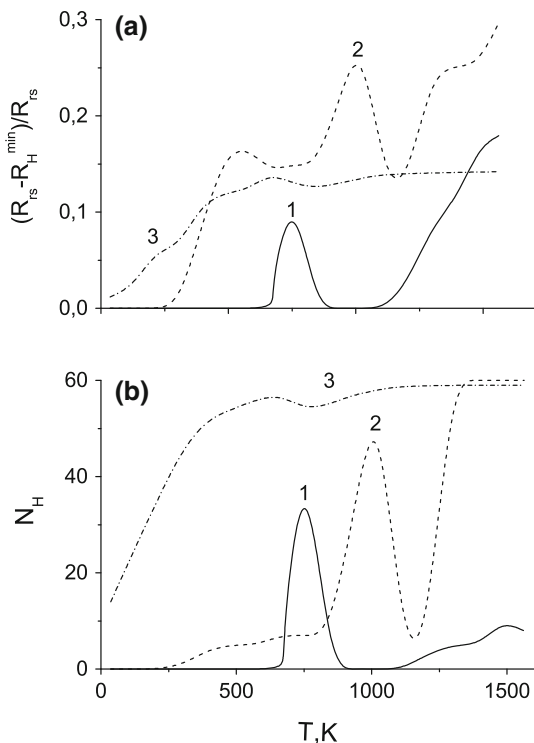


Fig. 6 Temperature dependences of **a** the relative depth of penetration of hydrogen atoms into the Si_{73} clusters, and **b** the number of hydrogen atoms adsorbed on these particles. The number designations are the same as in Fig. 2

nanoassembled cluster has the smallest size, and the largest radius R_{rs} is observed for the nanocrystal.

The degree of penetration of hydrogen atoms into the cluster can be defined as the ratio $\xi = (R_{cl} - R_H)/R_{rs}$, where R_H is the distance from the center of mass of the silicon cluster to the hydrogen atom nearest to the center of mass. The temperature dependence $\xi(T)$ for the nanoassembled cluster exhibits a maximum at 746 K, and the degree of penetration ξ , beginning with 1,100 K increases progressively (Fig. 6a). Two peaks are observed in the temperature range $0 \leq T \leq 1,150$ K in the dependence $\xi(T)$ for the nanocrystal. The highest peak is located at a temperature of 1,004 K. An increase in the temperature to 1,165 K is accompanied by a monotonic increase in the quantity ξ , for the nanocrystal. The temperature dependence $\xi(T)$ for the cluster with the random atomic packing is rather smooth. However, this dependence also exhibits a small maximum at $T = 690$ K. The locations of all

the maxima at the above temperatures coincide with those in the corresponding dependences $R_{rs}(T)$.

The temperature dependences of the number of hydrogen atoms (N_H) located in the spherical layer of thickness $(R_{rs} - R_H)$ for the clusters are depicted in Fig. 6b. Among the clusters under investigation, the Si_{73} nanoassembled cluster has the smallest value of N_H . The maximum number $N_H = 33$ is observed at a temperature of 746 K immediately before the evaporation temperature. After subsequent heating of the cluster by ~ 90 K, the number N_H becomes equal to zero. At temperatures above 1,090 K, this quantity insignificantly increases to $N_H = 9$. The dependence of the number N_H for the nanocrystal exhibits a maximum at $T = 1,004$ K ($N_H = 47$). However, already after the next heating stage, the number N_H decreases to 6. At a temperature of 1,350 K, the number N_H becomes equal to 60, i.e., all the H atoms are located in the surface nanocrystal layer of thickness $(R_{rs} - R_H)$. The dependence $N_H(T)$ for the cluster with the random atomic packing is characterized by a considerably smoother behavior. In this dependence, there is a small maximum ($N_H = 55$) at the temperature $T = 690$ K. The next extremum (minimum) turns out to be not deep ($N_H = 52$), and the quantity N_H at the temperature $T = 1,000$ K reaches almost a maximum value ($N_H = 59$).

Structure of Si_{60} clusters in the presence of hydrogen

The effect of hydrogen on the shape and structure of the Si_{60} cluster is illustrated in Fig. 7, where the configuration of the Si_{60} cluster without hydrogen and with hydrogen inside and outside the cluster at the temperature 1,500 K at the time instant 100 ps is shown. The H atoms initially placed inside the fullerene are marked by crosses within circles, and the H atoms arranged outside the Si cluster at the time $t = 0$, i.e., before the basic run at $T = 10$ K, are shown by open circles. It is evident that the volume of the cluster in vacuum (Fig. 7a) is much larger than the volume of the Si_{60} fullerene filled with 60 H atoms and surrounded with the same number of H atoms on the outside (Fig. 7b). Evaporated Si atoms are present in both cases; however, in vacuum, these Si atoms are separated from the cluster by larger distances. In addition, the Si cluster placed in the

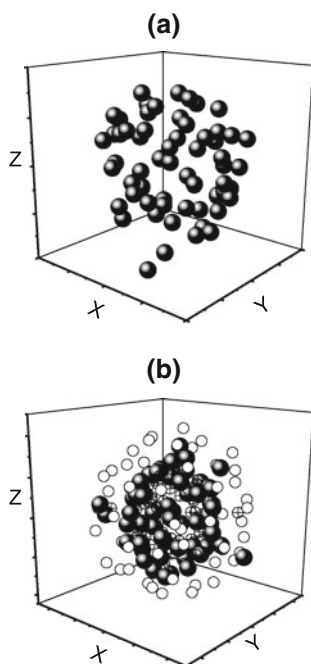


Fig. 7 Atomic configuration of the silicon fullerene at the temperature 1,500 K **a** in vacuum and **b** in a hydrogen “coat” in addition to 60 hydrogen atoms filling the interior space

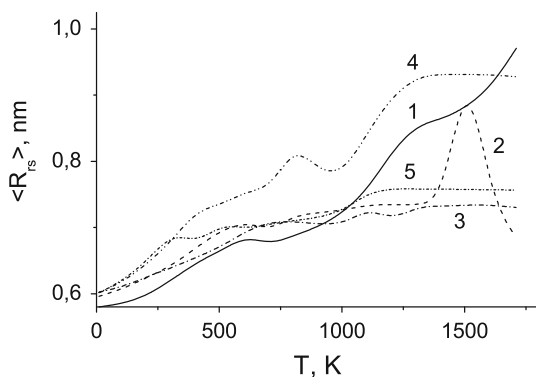


Fig. 8 The radius R_{rs} of the restricting sphere for silicon fullerene in the conditions of (1) vacuum, (2, 3) compensation of unpaired Si bonds by (2) 30 and (3) 60 H atoms inside the fullerene, and (4, 5) coating with H atoms and filling of the interior space of the fullerene with (4) 30 and (5) 60 H atoms

hydrogen medium better retains spherical shape and a more homogeneous distribution of the constituent atoms over the spherical surface. Thus, the positive role of hydrogen in stabilizing the shape and structure of the Si_{60} cluster is obvious. Nevertheless, it is found that, even in the hydrogen environment, the silicon fullerene is not quite stable and loses its atoms with

increasing temperature. It is also worth noting that some H atoms initially located inside the cluster (at $T = 10$ K) escape from the cluster to the outside.

In the calculations we traced the effective cluster size by determining the radius R_{rs} of the restricting sphere that includes all Si atoms which are at a distance of $r \leq r_2$ to the nearest atom. For the whole series of calculations, the number of atoms that evaporated from the Si_{60} cluster during the observation time of 100 ps was no larger than three. The temperature dependences of the R_{rs} in five series of the calculations for the Si cluster (in the presence and absence of hydrogen) are shown in Fig. 8. In general, the quantity R_{rs} increases with increasing temperature in all cases. It is connected to observably evaporation of atoms Si from clusters. The effective size of cluster R_{rs} is not true radius of cluster because it can characterize cluster with evaporating Si atoms. Here the moment of evaporation of Si atom from cluster precisely is not established. Besides the evaporating atom can keep in contact with cluster through hydrogen atoms. The dependence $R_{rs}(T)$, as a rule, exhibits peaks. Such peaks are clearly pronounced in dependences 2 (1,510 K) and 4 (820 K), i.e., in the case of 30 H atoms inside the cluster surrounded and not surrounded with external hydrogen. In the temperature range $10 \text{ K} \leq T \leq 1,711 \text{ K}$, the parameter R_{rs} shows a most profound increase if the cluster is in vacuum (dependence 1); the smallest values of R_{rs} are obtained in the case of 60 H atoms inside the cluster (dependence 3). A slight increase in R_{rs} at high temperatures can also be seen for the cluster with 60 H atoms inside and outside the cluster (dependence 5). The cluster size is found to be unstable if there are 30 H atoms inside the cluster (dependences 2, 4). In this case, if such a cluster is surrounded by 60 H atoms on the outside (dependence 4), the radius R_{rs} has the largest values compared to R_{rs} obtained in the other series of calculations for the temperature range $310 \text{ K} \leq T \leq 1,630 \text{ K}$.

Parameters of the Si–Si bonds in Si_{60} clusters stabilized with hydrogen

The temperature variations in the number of bonds per atom, \bar{n}_b , and in the average bond length, \bar{L}_b , are shown in Fig. 9. At low temperatures (below ~ 500 K), the parameter \bar{n}_b remains unchanged or

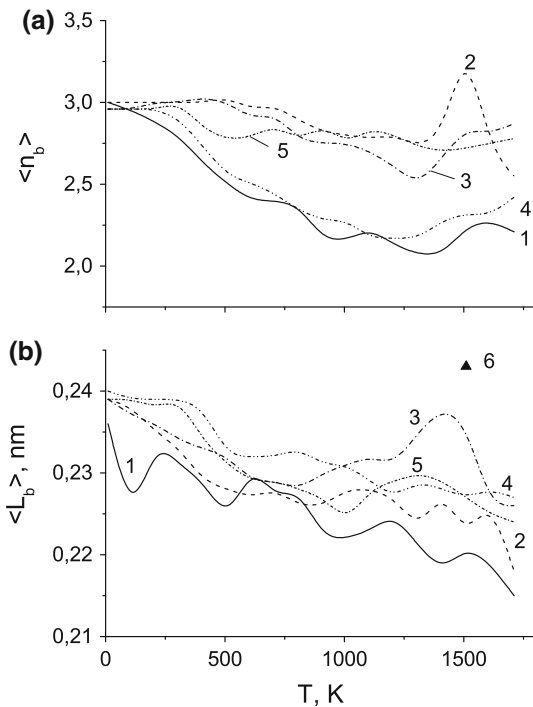


Fig. 9 Temperature dependences of **a** the average number of bonds per atom \bar{n}_b and **b** the average Si–Si bond length \bar{L}_b for the Si₆₀ fullerene. The numbers of curves 1–5 correspond to the same conditions as in Fig. 8. Symbol 6 refers to the result of molecular dynamic simulation for the Si₂₀₀ nanoparticle (Hawa and Zachariah 2004)

slightly increases for the Si₆₀ cluster filled with H atoms and not surrounded with a hydrogen “coat”; for the other fullerenes, \bar{n}_b decreases. However, as the temperature is increased further, the quantity \bar{n}_b decreases for all clusters. The quantity \bar{n}_b reduces most dramatically if the cluster is in vacuum (dependence 1) and if there are 30 H atoms inside the cluster and 60 H atoms outside (dependence 4). The quantity \bar{n}_b is most stable for the Si cluster filled and surrounded with 60 H atoms (dependence 5). In this case, in the entire temperature region, the quantity \bar{n}_b does not go below 2.7. Both with and without hydrogen in the vicinity of Si cluster, the values of \bar{n}_b are no larger than 3.2.

In the Si cluster, the average bond length \bar{L}_b decreases with increasing temperature (Fig. 9b). The parameter \bar{L}_b exhibits the most substantial decrease ($\sim 9\%$) in the cluster placed in vacuum (dependence 1). At high temperatures, the largest values of \bar{L}_b are exhibited by the cluster, within which there are

60 H atoms (dependence 3). The most stable quantity \bar{L}_b is typical of the Si clusters surrounded with hydrogen, with the interior space filled with H atoms (dependences 4, 5). In this case, if there are 30 H atoms inside the cluster, the parameter \bar{L}_b exhibits a 5% decrease in the temperature range $10 \text{ K} \leq T \leq 1,711 \text{ K}$; if there are 60 H atoms inside the cluster, the reduction of \bar{L}_b is 6%.

In Fig. 9b, symbol 6 refers to the Si–Si bond length in the Si₂₀₀ cluster, whose surface was covered by a hydrogen monolayer of 74 atoms (Hawa and Zachariah 2004). To simulate the Si–Si interactions, the authors of (Hawa and Zachariah 2004) used modified Stillinger–Weber’s potential (Stillinger and Weber 1985). The Si–H and H–H interactions were described by Kohen–Tully–Stillinger’s potential (Kohen et al. 1998). The Si₂₀₀ cluster presented a small part of a continuous, i.e., voids-free material. In the Si₂₀₀ cluster at 1,500 K, the average Si–Si bond length (0.243 nm) is larger than \bar{L}_b of the Si crystal.

If the fullerene is placed in vacuum or if there are 30 H atoms inside the fullerene and it is surrounded with a hydrogen “coat,” the quantity \bar{n}_b shows a sharp decrease in the temperature range from 10 to 1350 K. If there is no hydrogen, the decrease in \bar{n}_b is accompanied by a sharp decrease in the average bond length \bar{L}_b . Under temperature variations, the function $\bar{L}_b(T)$ oscillates. The well-pronounced maxima in the dependence $\bar{L}_b(T)$ for series 7 correspond to the temperatures 241, 630, 1195, and 1,528 K.

It should be noted that, for the cluster without hydrogen, there is a temperature range, $710 \text{ K} \leq T \leq 800 \text{ K}$, in which the quantity \bar{L}_b stops decreasing. At the temperature 773 K, Khokhlov et al. (1998a, b) annealed *a*-Si films with thicknesses from 100 to 500 nm; as a result, a new modification of silicon, silicyne, was produced. Silicyne consists of linear atomic chains that show sharp bends at every 5–10 atoms. In the chains, the constituent atoms have two Si–Si bonds, while at the bends, the atoms have three Si–Si bonds. The average number of Si–Si bonds per atom in silicyne is close to the number \bar{n}_b obtained here for the Si fullerene at $T > 789 \text{ K}$ in series 1 and 4 (Fig. 9a). In Fig. 6a, the chains of 2–5 Si atoms can be seen, and along with the chains there are three-dimensional clouds of atoms. Thus, when the fullerene is broken down at high temperatures, linear chains of atoms are formed. Similar chains are involved in the silicyne structure.

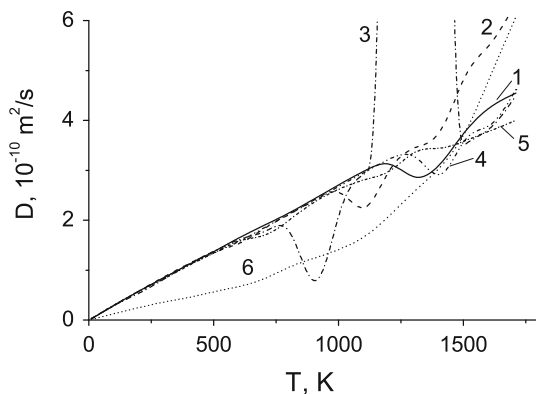


Fig. 10 The temperature dependence of the self-diffusion coefficient in the Si_{60} fullerene. The numbers of curves 1–5 correspond to the same conditions as in Fig. 8. Curve 6 refers to the result of molecular dynamic simulation for the Si_{200} nanoparticle (Hawa and Zachariah 2004)

Coefficients of diffusion and linear expansion

The mobility of atoms in the hollow clusters studied here is illustrated in Fig. 10. At low temperatures (up to 550 K), hydrogen does not produce any noticeable effect on the self-diffusion coefficient D of Si atoms. All five series of calculations give virtually the same dependence $D(t)$. The noticeable influence of hydrogen on the kinetics of Si atoms is observed at $T > 770$ K. Particularly profound changes in D occur for the Si cluster containing 60 H atoms in the interior space. At first, the pressure created by hydrogen reduces the mobility of atoms in silicon, and then the quantity D sharply increases due to evaporation of Si atoms. For this cluster at $T \sim 1,500$ K, the quantity D follows again the dependence $D(t)$ for the clusters treated in series 1, 4, and 5. When the number of H atoms inside the Si cluster is half of that in series 3, i.e., equal to 30 (dependence 2 in Fig. 10), a sharp increase in the dependence $D(t)$ can be seen at higher temperatures, starting from $\sim 1,370$ K; this increase is also due to evaporation of Si atoms. If there is hydrogen inside and outside the cluster (series 4, 5), we can see oscillations of the function $D(t)$ at $T > 1180$ K. In this case, equalization of the numbers of H atoms inside and outside the Si cluster suppresses the oscillations of $D(t)$ at high temperatures. For the Si cluster in vacuum (dependence 1) at $T > 1,180$ K, the function $D(t)$ oscillates with an

amplitude even larger than that for dependences 4 and 5 in Fig. 10.

Curve 6 in Fig. 10 is the result of MD calculations (R sibois and De Leener 1977) of the self-diffusion coefficient of the Si nanoparticle consisting of 6,400 atoms. At the surface of that cluster, there was a monolayer of 785 H atoms. In contrast to the S_{60} cluster studied here, the S_{6400} cluster was free of voids. It can be seen that, in the temperature range $10 \text{ K} \leq T \leq 1,350 \text{ K}$, the self-diffusion coefficient of the S_{6400} nanoparticle, as a rule, is noticeably smaller than the corresponding coefficient D of the clusters considered in this study. However, at $T > 1500 \text{ K}$, the increase in the coefficient D of the S_{6400} nanoparticle becomes steeper than the increase in D of the clusters considered here. This is most likely due to the Stillinger–Weber potential used to describe the Si–Si interactions in the nanoparticles. This potential provides a coefficient D larger than those obtained with the potential used here because of the substantially higher mobility of surface atoms at a high temperature.

The estimation of the linear expansion coefficient β for the S_{60} cluster in the temperature range 511–611 K shows that the Si fullerene filled with 60 H atoms exhibits the largest value of β ($6.09 \times 10^{-5} \text{ K}^{-1}$), while the S_{60} cluster covered with hydrogen shells of 60 atoms features the smallest value ($-1.51 \times 10^{-5} \text{ K}^{-1}$). The negative value of β shows that, in the latter case, we have interplay of various factors associated with the pressure produced by hydrogen both inside and outside the cluster and with the surface tension of the fullerene in vacuum. In vacuum, the Si fullerene that has kinetic energy corresponding to the temperature 561 K is characterized by a coefficient β at least an order of magnitude larger than the average value of β ($3.5 \times 10^{-6} \text{ K}^{-1}$) for crystalline silicon (Shelykh et al. 2006a, b) at the same temperature.

Conclusion

The results of the computer experiment demonstrated that the Si_{73} clusters well adsorb hydrogen at low temperatures. The hydrogen “coat” is retained around these particles up to high temperatures ($\sim 1,500$ – $1,600 \text{ K}$). The nanoparticle composed of

the icosahedron and the fullerene retains the highest density up to a temperature of 1560 K. The nanoassembled particle has the most stable number (close to four) of Si–Si bonds per atom in the temperature range $35 \leq T \leq 1,560$ K. In each investigated particle, the constraining sphere size R_{rs} increases with the temperature. In calculations using canonical ensemble the temperature changes of magnitudes \bar{n}_b and \bar{L}_b appear more essential, than in case of their definition with the help of microcanonical ensemble. Moreover, the particle shape does not deviate significantly from a spherical shape. As a result, holes should be formed inside the particles, and these holes can be occupied by hydrogen. The practical importance of our investigation is associated with the use of hydrogen as a fuel.

The calculations show that the Si₆₀ fullerene is not a stable cluster, as can happen with its C₆₀ analogue. At low temperatures, the Si₆₀ fullerene placed in vacuum collapses, which is promoted by the formation of short chains and small bulk fragments and by the decrease in the average bond length. At high temperatures, the broken Si₆₀ fullerene increases its initial volume, and a fraction of the constituent atoms evaporate, whereas the remaining atoms are grouped into chains and ultrasmall clusters consisting of several (2–8) atoms. At lower temperatures ($100 \text{ K} \leq T \leq 800 \text{ K}$), the complete compensation of unpaired Si–Si bonds with hydrogen inside the fullerene produces the effect of diffusion “resistance”; in this case, the self-diffusion coefficient is nearly halved. In addition to the filling of the fullerene interior space with hydrogen, the creation of a hydrogen “coat” outside the fullerene tends to decrease the probability of evaporation of Si atoms, but does not protect the system from a sharp decrease in the number of bonds per atom at high temperatures. At a temperature close to 270–280 K, the Si₆₀ fullerene filled with 60 hydrogen atoms and covered with a hydrogen “coat” is close to the boundary of thermal stability.

Thus, the conclusion can be drawn that the computer simulation makes it possible to predict the structure and physical properties of new noncrystalline materials and to improve the technology used for their production. Among the group IV elements, the perfect icosahedral symmetry is unique to carbon whose smaller covalent radius generates sufficient strain to overcome any gain in energy by forming structures with large coordination.

Acknowledgements This study was supported by the Presidium of the Ural Division of the Russian Academy of Sciences within the framework of the Integration Project of the Ural Division–Far East Division of the Russian Academy of Sciences.

References

- Berendsen HJC, Postma JPM, van Gunsteren WF, DiNola A, Haak JR (1984) Molecular dynamics with coupling to an external bath. *J Chem Phys* 81:3684–3990
- Biswas P, Hamman DR (1987) New classical models for silicon structural energies. *Phys Rev B* 36:6434–6445
- Endo RK, Fujihara Y, Susa M (2003/2007) Calculation of density and heat capacity of silicon by molecular dynamics simulation. *High Temp High Press* 35/36: 505–511
- Ferraro MB (2007) Prediction of structures and related properties of silicon clusters. *J Comp Meth Sci Eng* 7:195–217
- Galashev AE, Polukhin VA, Izmodenov IA, Rakhmanova OR (2007) Molecular dynamics simulation of the physicochemical properties of silicon nanoparticles containing 73 atoms. *Glass Phys Chem* 33:86–95
- Hawa T, Zachariah MR (2004) Internal pressure and surface tension of bare and hydrogen coated silicon nanoparticles. *J Chem Phys* 121:9043–9049
- Hirschman KD, Tsybeskov L, Duttagupta SP, Fauchet PM (1996) Silicon-based visible light-emitting devices integrated into microelectronic circuits. *Nature (Lond)* 384:338–341
- Hiura H, Miyazaki T, Kanayama T (2001) Formation of metal-encapsulating Si cage clusters. *Phys Rev Lett* 86: 1733–1736
- Ho KM, Shvartsburg AA, Pan B, Lu Z-Y, Wang CZ, Wachter JG, Fye JL, Jarrold MF (1998) Structures of medium-sized silicon clusters. *Nature (Lond)* 392:582–583
- Honea EC, Ogura A, Peale DR, Felix C, Murray CA, Raghavachari K, Sprenger WO (1999) Structures and coalescence behavior of size-selected silicon nanoclusters studied by surface-plasmon-polariton enhanced Raman spectroscopy. *J Chem Phys* 110:12161–12171
- Khokhlov AF, Mashm AI, Khokhlov DA (1998a) New allotropic form of silicon. *Pis'ma Zh EkspTeor Fiz* 67: 646–649
- Khokhlov AF, Mashm AI, Khokhlov DA (1998b) New allotropic form of silicon. *JETP Lett* 67:675–678
- Kohen D, Tully JC, Stillinger FH (1998) Modeling the interaction of hydrogen with silicon surfaces. *Surf Sci* 397:225–236
- Kwon I, Biswas R, Soukoulis CM (1992) Molecular-dynamics simulations of defect formation in hydrogenated amorphous silicon. *Phys Rev B* 45:3332–3339
- Li BX, Cao PL (2000) Stable structures for Si₂₀ clusters. *Phys Rev A* 62: 023201 (1–5)
- Li B-X, Cao P-L (2001) Distorted cage structures of Si_n (n = 20, 24, 26, 28, 30, 32) clusters. *J. Phys* 13: 10865–10872
- Li B-X, Cao P-L, Songa B, Yea Z-Z (2003) Stability of neutral and charged Si₅₀ cage and stacked structure and in comparison with Si₆₀ structures. *J Mol Struct* 620:189–196

- Mousseau N, Lewis LJ (1991) Dynamical models of hydrogenated amorphous silicon. *Phys Rev B* 43:9810–9817
- Ohara M, Koyasu K, Nakajima A, Kaya K (2003) Geometric and electronic structures of metal (M)-doped silicon clusters (M = Ti, Hf, Mo and W). *Chem Phys Lett* 371:490–497
- Rechtsteiner GA, Hampe O, Jarrold MF (2001) Synthesis and temperature-dependence of hydrogen-terminated silicon clusters. *J Phys Chem B* 105:4188–4194
- Résibois P, De Leener M (1977) *Classical kinetic theory of fluids*. Interscience, New York
- Shelykh AI, Smirnov BI, Smirnov IA, de Arellano-Lopez AR, Martinez-Fernandez J, Varela-Faria FM (2006a) Coefficient of linear expansion of the biomorphous composite SiC/Si. *Fiz Tverd Tela* 48:202–203
- Shelykh AI, Smirnov BI, Smirnov IA, de Arellano-Lopez AR, Martinez-Fernandez J, Varela-Faria FM (2006b) Coefficient of linear expansion of the biomorphous composite SiC/Si. *Phys Solid State* 48:216–217
- Stillinger FH, Weber TS (1985) Computer simulation of local order in condensed phases of silicon. *Phys Rev B* 31:5262–5271
- Sun Q, Wang Q, Jena P, Yu JZ, Kawazoe Y (2003) Geometry and energetics of Si₆₀ isomers. *Sci Tech Adv Mat* 4:361–365
- Tersoff J (1988) New empirical approach for the structural and energy of covalent systems. *Phys Rev B* 37:6991–7000
- Tersoff J (1989) Modeling solid-state chemistry: interatomic potentials for multicomponent systems. *Phys Rev B* 39:5566–5568
- Watanabe M, Adachi M, Morishita T, Higuchi K, Kobatake H, Fukuyama H (2007) Does supercooled liquid Si have a density maximum? *Roy Soc Chem Faraday Discuss* 136:279–286
- Yin MT, Cohen ML (1982) Theory of static structural properties, crystal stability, and phase transformations: application to Si and Ge. *Phys Rev B* 26:5668–5687
- Yoo S, Zeng XC, Zhu X, Bai J (2003) Possible lowest-energy geometry of silicon clusters Si₂₁ and Si₂₅. *J Am Chem Soc* 125:13318–13319
- Yu B, Meyyappan M (2006) Nanotechnology: role in emerging nanoelectronics. *Solid-State Electron* 50:536–544